11-5-2020

Selective One-Dimensional ^{13}C-^{13}C Spin-Diffusion Solid-State Nuclear Magnetic Resonance Methods to Probe Spatial Arrangements in Biopolymers including Plant Cell Walls, Peptides, and Spider Silk

Bennett Addison
Renewable Resources and Enabling Sciences Center

Dillan Stengel
San Diego State University

Vivek S. Bharadwaj
Renewable Resources and Enabling Sciences Center

Renee M. Happs
Renewable Resources and Enabling Sciences Center

Crissa Doeppke
Renewable Resources and Enabling Sciences Center

Recommended Citation

Addison, B., Stengel, D., Bharadwaj, V., Happs, R., Doeppke, C., Wang, T., Bomble, Y., Holland, G., & Harman-Ware, A. (2020). Selective One-Dimensional ^{13}C-^{13}C Spin-Diffusion Solid-State Nuclear Magnetic Resonance Methods to Probe Spatial Arrangements in Biopolymers including Plant Cell Walls, Peptides, and Spider Silk. *Journal of Physical Chemistry B, 124* (44), 9870-9883. https://doi.org/10.1021/acs.jpcb.0c07759

Selective 1D ^{13}C-^{13}C Spin-Diffusion Solid-State NMR Methods to Probe Spatial Arrangements in Biopolymers Including Plant Cell Walls, Peptides and Spider Silk

Bennett Addison[*a], Dillan Stengel[c], Vivek S. Bharadwaj[a], Renee M. Happs[a], Crissa Doeppke[a], Tuo Wang[d], Yannick J. Bomble[b], Gregory P. Holland[†c], Anne E. Harman-Ware[†a]*

*Corresponding Author: bennett.addison@nrel.gov
[†]Designates co-senior authors

AUTHOR ADDRESS

[a]Renewable Resources and Enabling Sciences Center, 15013 Denver West Parkway, Golden, Colorado 80401, USA
[b]Biosciences Center, 15013 Denver West Parkway, Golden, Colorado 80401, USA
[c]Department of Chemistry and Biochemistry, San Diego State University, San Diego, CA, 92182-1030, USA
[d]Department of Chemistry, Louisiana State University, Baton Rouge, LA 70803, USA

KEYWORDS: Solid-state NMR, DARR, DARR Difference, DANTE Difference, Spin diffusion, Biomass, Cell Wall, Lignocellulose, Lignin, Xylan, Polysaccharide, Spider silk

ABSTRACT

2D and 3D through-space ^{13}C-^{13}C homonuclear spin-diffusion techniques are powerful solid-state NMR tools for extracting structural information from ^{13}C-enriched biomolecules, but necessarily

long acquisition times restrict their applications. In this work we explore the broad utility and underutilized power of a chemical shift-selective One-Dimensional (1D) version of 2D ^{13}C-^{13}C spin-diffusion solid-state NMR technique. The method, which is called 1D DARR Difference, is applied to a variety of biomaterials including lignocellulosic plant cell walls, microcrystalline peptide fMLF, and Black Widow dragline spider silk. 1D ^{13}C-^{13}C spin-diffusion methods described here apply in select cases in which the 1D ^{13}C solid-state NMR spectrum displays chemical-shift resolved moieties. This is analogous to the selective 1D NOESY experiment utilized in liquid-state NMR as a faster (1D instead of 2D) and often less ambiguous (direct sampling of the time-domain data, coupled with increased signal averaging) alternative to the 2D NOESY. Selective 1D ^{13}C-^{13}C spin-diffusion methods are more time-efficient than their 2D counterparts such as Proton-Driven Spin Diffusion (PDSD) and Dipolar-Assisted Rotational Resonance (DARR). The additional time gained enables measurements of ^{13}C-^{13}C spin-diffusion buildup curves and extraction of spin-diffusion time constants T_{SD}, yielding detailed structural information. Specifically, selective 1D DARR Difference buildup curves applied to ^{13}C-enriched hybrid poplar woody stems confirm strong spatial interaction between lignin and acetylated xylan polymers within poplar plant secondary cell walls, and an inter-polymer distance of ~0.45 – 0.5 nm was estimated. Additionally, Tyr/Gly long-range correlations were observed on isotopically enriched Black Widow spider dragline silks.

INTRODUCTION

Solid-state NMR spin-diffusion methods are powerful tools for investigating structural and architectural features of a wide variety of biomaterials. Particularly useful are multi-dimensional ^{1}H-mediated ^{13}C-^{13}C through-space correlation experiments, such as the 2D proton-driven spin-

diffusion (PDSD) and 2D Dipolar-Assisted Rotational Resonance (DARR) methods.[1-3] In general, these experimental schemes often start with the creation of ^{13}C traverse magnetization using a ^{1}H-^{13}C cross-polarization step followed immediately by a t_1 evolution period to encode ^{13}C chemical shifts in the indirect dimension. Magnetization is then stored along the z axis to enable ^{13}C-^{13}C spin-diffusion. During a variable spin-diffusion mixing period (τ_m), PDSD can be applied, which passively reintroduces ^{1}H-^{13}C dipolar coupling by turning off the decoupling power. To improve the efficiency of polarization transfer, ^{1}H-assisted recoupling techniques (such as DARR, PARIS, and CORD) can be employed to actively re-introduce the ^{1}H-^{13}C dipolar couplings that have been attenuated by magic-angle spinning (MAS).[3-7] Data is collected after a final ^{13}C readout pulse. These 2D (or occasionally 3D) through-space ^{13}C correlation experiments provide key structural information by revealing through-space contacts between ^{13}C nuclei; the presence of off-diagonal cross-peaks indicate ^{13}C nuclei that exchange spin polarization via the dipolar coupling interaction, hence the term ^{13}C-^{13}C spin-diffusion.

Since the time constant that governs the rate of ^{13}C-^{13}C spin exchange, T_{SD}, is proportional to the square of the strength of the dipolar coupling interaction between the two nuclei, these spin-diffusion measurements inherently contain internuclear distance information with a loose $1/r^6$ relation.[2, 8-10] For this reason, 2D PDSD or DARR datasets are commonly collected using a range of spin-diffusion periods between short (~1 - 100 ms, upper limit of ~0.3 nm), medium (~100 - 500 ms, upper limit of ~0.3 - 0.5 nm) and long (> 500 ms, upper limit of ~0.5 - 1 nm).[11] Short-range correlations are key for assigning ^{13}C chemical shifts, which are used to determine the backbone dihedral angles and thus secondary structure of proteins[12-14] as well as to differentiate the diverse linkage patterns and torsional conformations of carbohydrates in lignocellulosic biomass.[15]

Equally important is the information learned from long-range spin-diffusion measurements. ^{13}C-^{13}C cross-correlations observed at long mixing times - but not at short contact times - are crucial for investigating 3-dimensional protein folding,[16-18] amyloid fibrils,[19-21] insect silks,[22, 23] membrane proteins,[24, 25] as well as probing polymer-polymer interactions in biomolecular complexes such as bones and plant and fungal cell walls.[26-30] These 2D / 3D techniques, while exceptionally powerful and ubiquitously applied to biomaterials, are time-consuming due to the multidimensional nature necessitating many scans. It is therefore challenging to observe weak long-range contacts due to the insufficient sensitivity. This is a larger problem for sparsely labeled materials in which the level of isotopic enrichment is low (see spider silk, later section).

Liquid-state NMR methods encounter a similar problem; weak ^{1}H-^{1}H through-space contacts are easily omitted in the 2D NOESY experiments without adequate signal averaging. To address this issue, selective 1D versions of the 2D NOESY have been implemented.[31-35] A chosen ^{1}H signal is selectively irradiated, and magnetization exchange that occurs between protons within close spatial proximity during the NOESY mixing period is detected by direct observation in the 1D time domain. If the ^{1}H signals of interest are resolvable, the 1D selective NOESY experiment is more meritorious over the 2D version because of the significantly faster data collection and the reduced ambiguity due to directly sampled time domain.

Conceptionally, in select cases 2D solid-state NMR methods could similarly be collapsed into 1D versions using selective measures. While selective radio-frequency pulse generation is commonplace in solution-state NMR pulse programs using modern NMR hardware (i.e., 1D Selective NOESY), selective pulses for solid-state NMR experiments are more challenging to execute and therefore are not routinely implemented. In the context of 1D ^{13}C-^{13}C ssNMR spin-diffusion experiments, a few relevant examples can be found. First, the seminal DARR paper from

Takegoshi et al. in 2001 used a soft rectangular pulse to selectively invert the CH_3 signal of ^{13}C-enriched DL-Valine, and then monitored the time-dependent magnetization exchange between the inverted CH_3 and the non-inverted C=O group during a variable spin-diffusion period under different recoupling conditions.[3] In a similar manner, improved selectivity can be achieved by replacing the single soft rectangular inversion pulse with the DANTE (**d**elays **a**lternating with **n**utation for **t**ailored **e**xcitation) block.[36] In this scheme, a series of short hard pulses are placed on resonance and separated by rotor-synchronized delays, which selectively inverts the chosen signal. This version of the 1D PDSD method was used to monitor spin-diffusion within bacterial cellulose.[37] In both of those cases however, the selectively inverted signal is phased negatively while all other signals are positively phased, like in Figure 1d. Interpretation of the time-dependent return of magnetization back to equilibrium is therefore nearly impossible for heterogeneous systems with overlapping resonances like lignocellulosic biomass. An example of data collected in this manner is shown in Supplemental Figure S1. In an attempt to circumvent these problems, Foston et al. studied ^{13}C-enriched corn stover with a 1D technique in which a lignin aromatic ^{13}C signal was selectively excited using the multi-hardpulse SELDOM[38] scheme and the ^{13}C-^{13}C spin-diffusion was monitored.[39] The SELDOM block selects a signal to retain while destroying unwanted magnetization after multiple cancelation cycles, reducing the spectral sensitivity. A more elegant approach to eliminate unwanted signal was first taken by the Schaefer group, in which a 1D selective inversion spin-diffusion experiment using the DANTE block is subtracted from a similar spectrum without inversion.[40] After subtraction, only signals involved in ^{13}C-^{13}C spin-diffusion with the selected resonance are observed. This technique was coined "Dante Difference" and has been applied in multiple forms by the pioneering group.[41-45] Since the DANTE inversion scheme utilizes a series of on-resonance short hard pulses, while easy to implement, it is

challenging to obtain a decent profile of selective inversion of the chosen peak without perturbing the other resonances. For biopolymers with signals that are not adequately resolved, other selection methods, for example using amplitude and phase-modulated shaped pulses with more "top-hat" like bandwidth profiles, might result in improvement.[46-48] As one example, Weber et al. used a Gaussian shaped inversion pulse to selectively invert lipid CH_3 signal, and spin-diffusion to nearby CH_2 sites was monitored over an array of DARR mixing times.[49]

Selective 1D [^{13}C-^{13}C] spin-diffusion methods, like the original 1D DARR[3], Dante Difference[40] and in our case the 1D DARR Difference method, are underutilized tools for probing molecular arrangements in biopolymers in rotating solids. We have successfully applied this method to a variety of ^{13}C-enriched biomolecules and biomaterials, including woody biomass, microcrystalline protein fMLF, and ^{13}C-enriched Black Widow spider dragline silk. Although the conceptual setup of 1D DARR Difference bears similarity to that of the Dante Difference technique, shaped pulses are implemented to achieve selective inversion as opposed to the DANTE block. Both methods were tested: our application utilizing shaped pulses has shown an obvious improvement in resolution and performance over the Dante Difference method, which was crucial for the lignocellulosic biomass (Figure S2). We show that selective 1D ^{13}C-^{13}C spin-diffusion methods are more time-efficient than conventional ssNMR 2D ^{13}C-^{13}C spin-diffusion experiments like PDSD and DARR, meaning similar information can be obtained in less time. One can alternatively implement up to two orders of magnitude more scan averages in the same timeframe. Importantly, with the interleaved data acquisition scheme 1D DARR Difference produces in-phase ^{13}C magnetization in which only signals involved in spin-diffusion with a chosen resonance are observed. Selective 1D spin-diffusion buildup plots and extracted spin-diffusion time constants yield detailed structural information. In an effort to demonstrate its spectroscopic power and broad

applicability across biopolymer types, highlighted here are careful analyses of 1D spin-diffusion buildup plots from ^{13}C-enriched poplar woody stems to estimate the spatial arrangements between lignin and xylan polymers within the secondary cell wall matrix, and applications to fMLF and spider dragline silk are also discussed. The detailed pulse program and operational guide have been provided to benefit the research community and facilitate future investigations on complex biomaterials.

EXPERIMENTAL METHODS

^{13}C Isotopic Enrichment and Harvesting of Poplar Stems

$^{13}CO_2$ (Sigma-Aldrich) was plumbed into a Percival Scientific (Perry, IA, USA) growth chamber at 700 ppm for ^{13}C isotopic labeling of plants. The growth chamber was not flushed prior to plant growth so as to not waste isotopically labeled carbon dioxide. DN34 hybrid poplar trees (approximately 12 inches high) were placed into the growth chamber for 4 weeks of growth under the following conditions: 16 hour day cycle from 8 am to 12 am, 23°C, 65% relative humidity, 700 ppm CO_2; 8 hour night cycle from 12 am to 8 am, 18°C, 65% relative humidity, 500 ppm $^{13}CO_2$. At the end of the labeling period, trees were approximately 18 inches high and were harvested. Leaves, stems, and roots were separated. Stems were debarked while wet and allowed to dry for several days on a benchtop prior to NMR analysis.

Solid-State NMR Experiments on Poplar Woody Stems. For clarity, in this manuscript the term 1D-DARR indicates the non-selective first slice of the conventional 2D DARR experiment, while 1D DARR-Difference implies selective inversion of a chosen resonance, and cancelation of unwanted signal via the described phase cycling scheme is executed to produce the difference spectrum. All solid-state NMR experiments collected on poplar biomass were performed on a 200

MHz (4.7 Tesla) Bruker Avance-IIIHD NMR spectrometer equipped with a Bruker 7 mm HX MAS probe. 40 mg of ^{13}C-enriched biomass (de-barked, milled to 40-mesh) was center-packed in a 7 mm zirconia MAS rotor with top and bottom teflon plugs. This restricted the sample to the center half of the NMR coil, which helped limit probe RF heterogeneity issues. Sample spinning speed was 7900 or 8000 Hz MAS for all measurements. Typical ^{1}H-^{13}C Cross Polarization (CP) conditions were: an initial 3 μs ^{1}H hard pulse followed by a CP spin-lock step where the ^{13}C radiofrequency field strength was held constant at 62 kHz and the ^{1}H field strength was matched to the +1 sideband using a 10% ramp. For 1D DARR Difference data, a hard ^{13}C storage pulse of 3.8 μs was used, followed by a Gaussian Cascade Q3[50] selective inversion 180° soft pulse to rotate a chosen resonance to -z. Selective inversion pulses were 7 ms, 12.5 ms, and 30 ms in duration for aromatic lignin, acetyl xylan and cellulose $^{c}C_4$ experiments, respectively, during which high power ^{1}H decoupling was applied. Selective inversion pulses were calibrated according to the procedure outlined in the header of the pulse sequence provided in the Supplemental Materials. During the spin-diffusion period τ_m, ^{1}H dipolar recoupling was re-introduced using a continuous wave RF pulse with the field-strength matched to the first rotor resonance condition, $\omega_r = \omega_1$. All experiments were collected using either 20480 (1D DARR Difference) or 2048 (1D-DARR) scans, a 3 second recycle delay, and a 300-ppm spectral window. High power ^{1}H decoupling (Bruker sequence swftppm-13) was applied during acquisition (10 ms), at a ^{1}H field-strength of 67 kHz. 20 Hz exponential line broadening was applied to each free induction decay before Fourier transform (MestreNova version 14). ^{13}C chemical shifts for biomass were referenced externally to TMS at 0.0 ppm (DSS at 2.01 ppm) by setting the downfield Adamantane signal to 38.48 ppm.[51] Resulting spectra were manually phased, baseline corrected, superimposed, and finally time-dependent magnetization data was extracted from stacked plots using the MestreNova built-in

Data-Analysis tool. T_1-compensation was achieved using a parallel 1D-DARR dataset (see discussion in Supplemental Materials). Final data analysis and curve fitting was performed using home-written Python scripts with the lmfit module.

Solid-State NMR Experiments on Microcrystalline fMLF and Black Widow dragline silk. All solid-state NMR experiments on fMLF and Black Widow (BW) dragline silk were performed using a 600 MHz (14.1 Tesla) Bruker AVANCE-IIIHD spectrometer equipped with a Bruker 1.9 mm HCN MAS probe. $^{13}C/^{15}N$ isotopically enriched microcrystalline fMLF was purchased from CortecNet Corp. Typical ^{1}H-^{13}C CP conditions used a 2.45 μs initial 90° pulse, followed by a CP spin-lock pulse where the ^{13}C field strength was held constant at 65 kHz and the ^{1}H field strength was matched to the +1 sideband using a 70-100% ramp. The contact time was limited to 250 μs since the CP buildup for protonated aromatic moieties occurs quickly. A 2.4 μs hard storage pulse was used to store ^{13}C magnetization along +z, followed by a selective inversion pulse of 6 ms (Gaussian Cascade Q3 shape) centered at the Phe aromatic ring resonance (131 ppm), during which high powered decoupling was applied. The selective inversion pulse was calibrated according to the procedure in the Supplemental Materials. For fMLF, 1D DARR Difference experiments were collected with 64 scans, while 2D DARR experiments were collected with 16 scans and 256 t1 points, both using a recycle delay of 5 seconds. T_1 compensation was achieved by measuring ^{13}C T_1 spin-lattice relaxation times for each peak using the Torchia method (Bruker pulse program cpxt1).[52] For Black Widow spider silk, all solid-state experiments used similar CP conditions as above. 1D DARR Difference experiments were collected with either 8192 scans, while 2D DARR experiments used 128 scans and 128 t1 increments. Both 1D and 2D experiments had a recycle delay of 4 s. To be consistent with the protein NMR literature, ^{13}C chemical shifts were referenced

externally to DSS at 0.0 ppm (TMS at -2.01 ppm) by setting the downfield adamantane signal to 40.49 ppm.[51]

To generate labeled silk, *Latrodectus hesperus* (Western Black Widow) spiders were immobilized and fed a saturated solution of uniformly-labeled (U-^{13}C/^{15}N) Ala and Phe while being forcibly silked at a constant rate of 2 cm/s as outlined by Work and Emerson.[53] Phe is metabolized to Tyr by the spider and incorporated into the silk.[54] After two weeks, 10.3 mg of silk was pooled and packed into a 1.9 mm rotor.

RESULTS AND DISCUSSION

Selective 1D ^{13}C-^{13}C Spin Diffusion Pulse Sequences

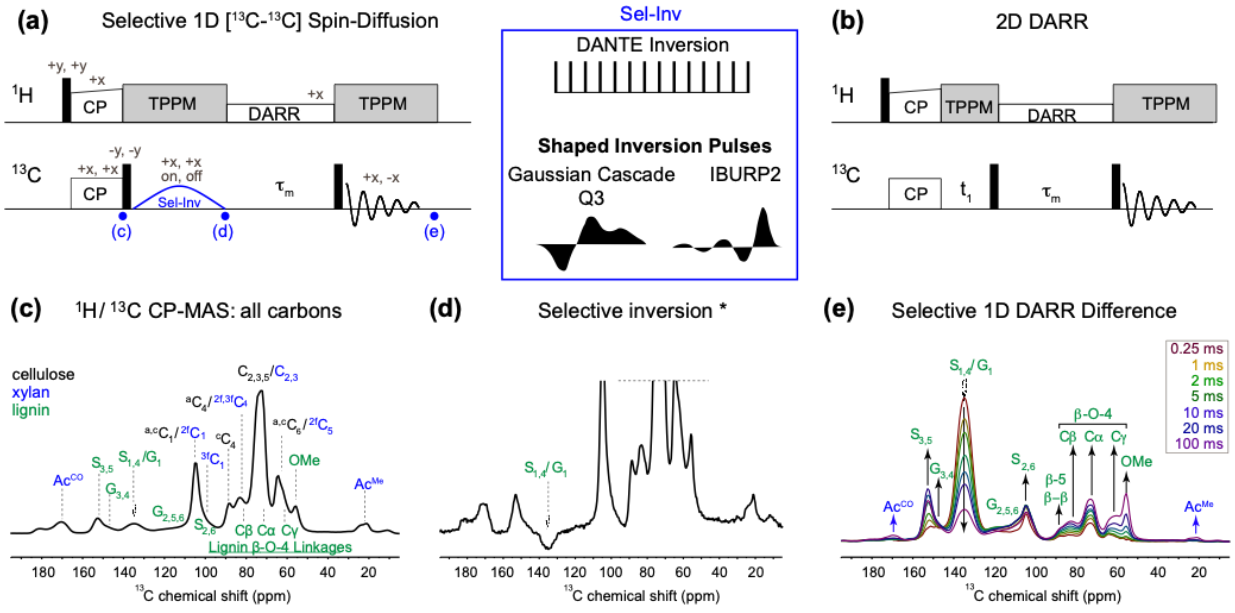

Figure 1. Pulse program for selective 1D ^{13}C-^{13}C spin-diffusion experiments, and its application to ^{13}C-enriched woody biomass. **(a)** Pulse program for 1D Dante Difference or 1D DARR Difference is displayed along with corresponding selective inversion schemes. **(b)** Pulse program for the 2D Dipolar-Assisted Rotational Resonance (DARR) experiment. The time points for collecting the spectra shown in Panel (c), (d), and (e) are highlighted in the pulse program. Selective 1D ^{13}C-^{13}C spin-diffusion experiments shown here begin with an initial ^{1}H excitation

pulse followed by a standard ^{1}H-^{13}C cross-polarization (CP) step **(c)**. A hard ^{13}C 90° pulse is then applied to store all ^{13}C magnetization along +z, followed by an optional z-filter. A selective inversion shaped soft pulse (Gaussian Cascade Q3 or IBURP) is then used to rotate a chosen resolved ^{13}C signal to -z. This pulse sequence becomes the Dante Difference method if the shaped pulse is replaced with the DANTE inversion block. If a readout pulse is applied immediately after the inversion pulse (asterisks signifies not implemented during 1D DARR Difference but used for setup and calibration), the selected ^{13}C peak should be phased negative while all other ^{13}C magnetization is phased positive **(d)**. Magnetization is allowed to equilibrate for a spin-diffusion period (τ_m between 0.25 – 100 ms displayed), in which spin exchange occurs with both the lattice and with nearby unequal spin-baths, with time constants given by T_1 and T_{SD}, respectively **(e)**.

The pulse sequence for 1D DARR Difference (and Dante Difference if one uses DANTE for inversion) selective 1D ^{13}C-^{13}C spin-diffusion experiments is illustrated in Figure 1a, along with the pulse program for the conventional Dipolar-Assisted Rotational Resonance (DARR) 2D ^{13}C-^{13}C correlation experiment (Figure 1b). 1D DARR Difference begins with a routine ^{1}H-^{13}C cross-polarization step to achieve ^{13}C polarization of all rigid moieties (Figure 1c). A ^{13}C hard pulse is then applied to store carbon magnetization along +z, followed by an optional z-filter. An amplitude and phase-modulated shaped selective inversion pulse (for example Gaussian Cascade or IBURP families)[50, 55] is applied every other scan to either invert (selection on) or leave unperturbed (selection off) a chosen resonance to -z while all other spins remain stored along +z (Figure 1d). High power ^{1}H decoupling is applied during this period to reduce ^{1}H-mediated ^{13}C-^{13}C spin-diffusion for the duration of the inversion pulse. After achieving selective inversion of a chosen signal to create chemical shift selected unequal ^{13}C spin baths, ^{1}H dipolar interactions are reintroduced through a low-power continuous wave RF pulse applied on the ^{1}H channel with power matched at the first rotor resonance condition ($\omega_r = \omega_1$) for a spin diffusion period τ_m, in a similar fashion to the mixing period in the 2D DARR. Alternatively, if no RF power is applied during the mixing period, the experiment becomes the selective 1D equivalent to the 2D PDSD method. If higher MAS spinning speeds are used, the DARR recoupling scheme could be easily replaced by recoupling programs better suited for higher MAS frequencies (CORD, AL FRESCO,

PARIS).[5-7, 56, 57] A ^{13}C hard pulse is then used to read out chemical shift selected spin-diffusion edited ^{13}C magnetization. Importantly, the receiver phase is alternated every other scan by 180°, matched with on and off-power selective pulses. In this way, we achieve fully in-phase ^{13}C magnetization for resonances involved in spin-diffusion with the selected signal, while other signals that are uninvolved in spin-diffusion are deconstructivity canceled through phase cycling. The end effect is similar to early implementations of Dante Difference experiments,[40, 43] but here cancelation of unwanted signal occurs directly by interleaving every other scan instead of through subtraction of two unique spectra. The pulse program displayed in Figure 1a notes the first two phase cycle conditions, but the full pulse program including a complete x y -x -y phase cycle and an optional rotor-synchronized echo prior to acquisition is included the Supplementary Materials.

Lignocellulosic Biomass: ***Isolation of Major Cell Wall Polymers from Poplar Woody Stems.***

Advanced ssNMR methods applied to ^{13}C-enriched lignocellulosic biomass in recent years have resulted in a significantly improved understanding of secondary cell wall superstructure.[26, 28, 58-61] This work demonstrates that selective 1D ^{13}C-^{13}C spin-diffusion experiments are also powerful ssNMR tools capable of extracting detailed structural information from ^{13}C-enriched heterogeneous materials like lignocellulosic biomass and spider silk. As illustrated in Figure 1c, the 1D ^{13}C CP-MAS spectrum of poplar woody stems gives rise to NMR signals from the three major polymers of lignocellulosic plant secondary cell wall: cellulose, hemicellulose and polyaromatic lignin. Clearly, significant overlap between many signals complicates analysis. The spectral overlap problem is usually alleviated with 2D and 3D techniques,[26, 28, 58-60] and indeed we have applied them successfully here (Figure 5a). But since some signals in the 1D CP-MAS spectrum can be exclusively assigned to a specific polymer (e.g., aromatic resonances arising primarily from lignin), 1D DARR Difference as a selective 1D spin-diffusion technique can be

applied to lignocellulosic biomass. Poplar hardwood is particularly well suited because 1) the mature woody biomass cell wall is composed nearly entirely of cellulose, lignin, and xylan existing mostly within the secondary wall, 2) the content of protein, metabolites and pectin are negligible, and 3) the composition of lignin and hemicellulose are well studied: i.e., poplar lignin is high in syringyl (S) and guaiacyl (G) lignin but low in p-hydroxyphenyl (H) and ferulate (FA) content, while hemicellulose is predominantly xylan with very little glucomannans.[62-64] Therefore, chemical shift selection of poplar lignin and hemicellulose domains can be achieved using the resonances of aromatics and acetyl groups (carbonyl and methyl motifs), respectively. Similarly, the cellulose microfibrils have a well-resolved peak at 89 ppm for crystalline cellulose $^{c}C_4$ (superscripts a and c denote amorphous and crystalline cellulose allomorphs, respectively). By collecting 1D DARR Difference data at short spin-diffusion times we could isolate the 1D ^{13}C ssNMR spectra of each of the three major cell wall polymers from in-tact biomass in its native and unaltered state. To the best of our knowledge this is the first time such a feat has been accomplished. Structural studies of individual cell wall components typically rely on chemical extraction procedures, which likely disrupt native molecular structures.[65-71] The resulting ^{13}C solid-state NMR spectra of isolated cell wall biopolymers are shown in Figure 2, and for context the CP-MAS spectrum is illustrated in grey below the cellulose sub-spectrum. It's notable that our best efforts to collect similar selective 1D spectra on biomass using the Dante Difference method were unsatisfactory compared to our specific implementation, likely due to improved control and selectivity of shaped pulses over the DANTE block for selective inversion (Supplemental Materials). This manuscript focuses primarily on data obtainable from the former.

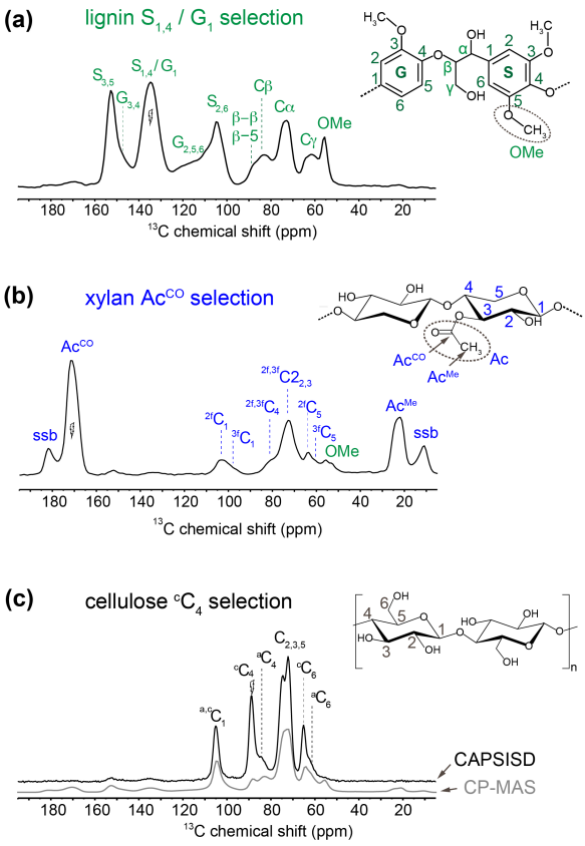

Figure 2. ^{13}C 1D DARR Difference solid-state NMR data on ^{13}C-enriched poplar biomass (50 MHz ^{13}C Larmor frequency, 7900 Hz MAS) revealing isolated ssNMR spectra of the three major plant cell wall polymers. (a) lignin-selected (20 ms, 135 ppm); (b) xylan-selected, (50 ms, 170 ppm); (c) cellulose-selected, (black, 50 ms, 89 ppm), with the CP-MAS spectrum in grey for perspective. Example chemical structures of each polymer are indicated with assignments.

Selection of lignin was achieved using a 7 ms Gaussian Cascade Q3 selective inversion pulse to isolate the lignin aromatic signal at 135 ppm, assigned to lignin $S_{1,4}$ / G_1 carbons. At this point, unequal nuclear spin populations exist with lignin $S_{1,4}$ / G_1 aligned along -z and all other signals aligned along +z (Figure 1d). Magnetization is then allowed to equilibrate during a variable spin-diffusion period, τ_m. At short spin-diffusion periods (1 – 100 ms, Figure 1e), the unequal distribution of ^{13}C spins has only partially equilibrated locally within the lignin nanodomains but has not yet diffused out to hemicellulose or cellulose polymers. Based on the idea that ^{13}C magnetization at short mixing times is restricted only to moieties immediately nearby the selected

lignin aromatic ring carbons, an isolated lignin sub-spectrum can be obtained from intact poplar stems after cancelation of any signals not involved in spin-diffusion.

The 20 ms lignin-selected 1D DARR Difference spectrum obtained from ^{13}C-enriched poplar is shown in Figure 2a. From this data, we can assign the ^{13}C chemical shifts of major lignin moieties, including sidechain linkages and methoxy decorations in the 50 - 90 ppm range, even though the chemical shifts of lignin linkages overlap significantly with carbohydrate signals. Chemical linkages between monomeric lignin units are dominated by β-O-4 structures.[62, 64] With relatively short spin-diffusion mixing times (1-100 ms), a clear buildup of broad and heterogeneous ^{13}C signals centered at 83, 73, and 62 ppm are observed (Figure 1e, 3a). These signals are assigned to lignin propyl sidechain Cβ, Cα, and Cγ environments, respectively (see Figure 2a chemical structure). Lignin methoxy carbons are easily identified at 56 ppm. All assignments taken from selective 1D data agree with the literature and are confirmed by 2D ^{13}C-^{13}C DARR methods (Figure 5a).[72-76] Assignments are summarized in Table S1.

Lignocellulosic Biomass: ***Spin-Diffusion Buildup Plots and Lignin/Polysaccharide Long-Range Contacts***

Lignin-selected T_1-compensated spin-diffusion buildup curves obtained from ^{13}C-enriched poplar woody stems are shown in Figure 3a. Data is plotted against the square root of the mixing time to better highlight spin-diffusion behavior at very long (3-7 seconds) mixing periods. We note that direct T_1 compensation is possible if the experiment is collected as the constant time version (z-filter plus mixing time sum to a constant),[42, 77] but this was not practical in the case of biomass so we used a supplemental non-selective 1D-DARR dataset to compensate for T_1. Further details of how T_1-compensated buildup plots were generated are described in the Supplemental Materials.

After selective inversion of the lignin $S_{1,4}$ / G_1 resonance at 135 ppm, ^{13}C magnetization is quickly lost to nearby spins and therefore the normalized intensity decays sharply (Figure 3a, 135 ppm). ^{13}C-enriched lignin moieties localized near the selected resonance quickly gain polarization as spin equilibration occurs within the lignin nanodomains. But at longer spin-diffusion periods (τ_m > 100 ms) ^{13}C magnetization further equilibrates outwards from lignin and towards other nearby polymers. This phenomenon of spin equilibration first within lignin then out to other domains is demonstrated nicely by monitoring the spin-diffusion behavior at 153 ppm (lignin $S_{3,5}$) and at 105 ppm (assigned to combination of lignin $S_{2,6}$, and polysaccharide C_1 moieties). Lignin equilibration is evident from the quick increase in the lignin $S_{3,5}$ resonance at 153 ppm (pre ~100 ms) followed by a decay at longer mixing times, while at 105 ppm the early buildup and prompt decay of magnetization is attributed to lignin $S_{2,6}$ moieties, and the lagging increase in signal at longer mixing times comes from spin-diffusion from lignin into polysaccharide domains (Figure 3a). The effects of T_1 relaxation have already been taken into account, so the decay of lignin ^{13}C magnetization after original buildup is due entirely to ^{13}C-^{13}C spin-diffusion from lignin domains outwards towards other sites within close proximity.

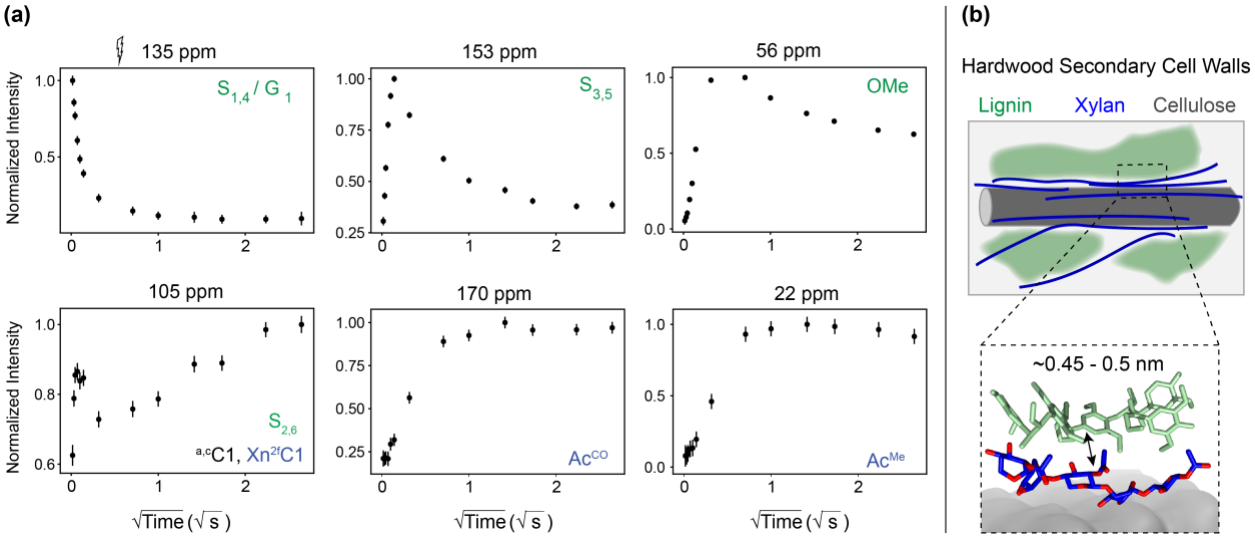

Figure 3: (a) Lignin-selected (135 ppm) T_1-compensated 1D DARR Difference buildup plots obtained on ^{13}C-enriched poplar biomass for select resonances. Data is plotted against the square root of the mixing times to better highlight spin-diffusion behavior at long τ_m. Curves were generated by processing the time-dependent change in ^{13}C magnetization according to Equation S4 using the non-selective 1D DARR dataset for T_1 compensation. Spin-diffusion time constants T_{SD} summarized in Table 1 were extracted from relevant buildup curves. Error bars directly arise from signal to noise ratios for each analyzed peak. **(b)** Likely hardwood secondary cell wall superstructure as revealed by selective 1D spin-diffusion buildup data shown in **(a)**.

At longer ^{13}C-^{13}C spin-diffusion mixing times, dipolar contact between lignin and nearby polysaccharides becomes clear. Lignin – hemicellulose polymer/polymer interactions are particularly obvious. The acetylated hemicellulose xylan gives rise to ^{13}C NMR signals at 22 ppm and 171 ppm for the acetyl CH_3 and CO groups, respectively (Figure 2b). Monitoring the T_1-compensated buildup behavior of these resonances therefore provides information on the spatial proximity of hemicellulose and lignin polymers. Figure 3a shows the T_1-compensated and normalized 1D DARR Difference spin-diffusion buildup curves for the Ac^{Me} and Ac^{CO} motifs in the acetyl groups in which magnetization originated at lignin aromatic ring sites (135 ppm). The curves demonstrate clear buildup behavior that is noticeably slower (longer T_{SD}, see Table 1) compared to the initial buildup rates observed for other lignin moieties (e.g., lignin $S_{3,5}$ signal at 153 ppm). This observation is consistent with finding hemicellulose at a distance farther away from the source (lignin $S_{1,4}$ / G_1) compared to other lignin moieties. The buildup rate of acetylated xylan is reasonably fast (320 – 380 ms) for an inter-polymer contact. Molecular Dynamics simulations of a model lignin oligomer facilitate estimations of key carbon-carbon distances that are physically realistic. They reveal that lignin methyl ether (-OMe) and sidechain Cγ are roughly 0.36 and 0.33 nm from relevant lignin ring moieties, respectively (Supplemental Figure S4). These sites were chosen as internal distance candles (or internal distance rulers) to estimate the average proton-driven ^{13}C-^{13}C spin-diffusion coefficient K under our acquisition conditions. The extracted T_{SD} buildup rates from the selected lignin aromatic signal to OMe and Cγ groups were 61 and 45

ms, respectively, which translated into a spin-diffusion coefficient K in the range of 2.9 $x10^{-5}$ nm^6/ms to $4.5x10^{-5}$ nm^6/ms. By applying the range of estimated spin-diffusion coefficients to xylan acetyl carbons, we extract an average inter-nuclear distance between lignin ring carbons and xylan acetyl groups of around 0.45 – 0.5 nm. A complete analysis of how this distance was estimated can be found in the Supplemental Materials. Therefore, for the first time we have experimentally measured the inter-polymer distance between the lignin and acetylated xylan surface within lignified plant cell walls. The data clearly suggests tight lignin-hemicellulose surface contact within the secondary cell walls of bioenergy-relevant poplar feedstock. Additionally, the carbohydrate signal at 105 ppm, assigned to hemicellulose and cellulose C_1 carbons, continues to build in even at very long (7 seconds) spin-diffusion mixing times. This indicates that carbohydrate moieties exist at a distance longer than ~1 nm from the lignin domains. Presumably part of the emerging signal at 105 ppm is from cellulose microfibrils.

Work from the Dupree lab has suggested that xylan from hardwoods might require acetyl group decoration every other xylose unit for cellulose binding (see Figure 2b structure),[78, 79] and it has been shown that cellulose-bound xylan adopts a 2-fold linearized conformation.[26, 59, 60] Therefore, acetyl groups from cellulose-bound xylan would all be pointing away from cellulose microfibrils towards the lignin-rich secondary cell wall matrix. The most plausible interpretation of the 1D DARR Difference spin-diffusion data is therefore the following: magnetization that begins in the lignin aromatic ring carbons first diffuses locally within the lignin nanodomains, and then to xylan acetyl Ac^{Me} and Ac^{CO} sites, as evident from the relatively fast buildup behavior of xylan acetyl groups. ^{13}C spin-diffusion then continues through the acetylated xylans, which are cellulose-bound, and finally magnetization penetrates into the cellulose microfibrils. Overall, these findings suggest that the secondary cell wall superstructure of poplar woody stems is consistent with the

secondary cell wall model proposed for hardwoods and grasses by Kang et al.[26] An illustration of this concept is presented in Figure 3b.

Application to microcrystalline protein fMLF. The selective 1D DARR Difference method was also applied to microcrystalline fMLF peptide, a common ssNMR standard sample. Data is shown in Figures 4 and 5, and additional data is presented in the Supplemental Materials. The standard CP-MAS spectrum (10 kHz MAS, 150 MHz ^{13}C Larmor frequency) is seen in Figure 4b along with the chemical structure and color-coded assignments for Met, Leu and Phe resonances. Selective 1D spectra were collected using the Phe aromatic ring carbons near 131 ppm for selection. At short mixing times, when ^{13}C-^{13}C spin-diffusion occurs mostly on a short length-scale, signals arising from Phe Cα, Cβ and CO emerge clearly while resonances from other residues are largely absent. While assigning Phe signals from the 50 ms spectrum (Figure 4c) is trivial just based on chemical shifts, one gains more confidence by analyzing the rate of magnetization transfer from Phe aromatic ring carbons to other ^{13}C sites. Select T_1-compensated buildup curves (10 kHz MAS) on fMLF are shown in Figure 4e. The spin-diffusion time constants extracted for Phe Cβ, Cα and CO were respectively 20, 47 and 74 ms, which correlate with proximity to the ring. Additionally, increasing spin-diffusion time constants extracted for Phe, Leu and Met carbonyl groups correlates with increasing distance from the Phe ring (Figure 4e, Table 1).

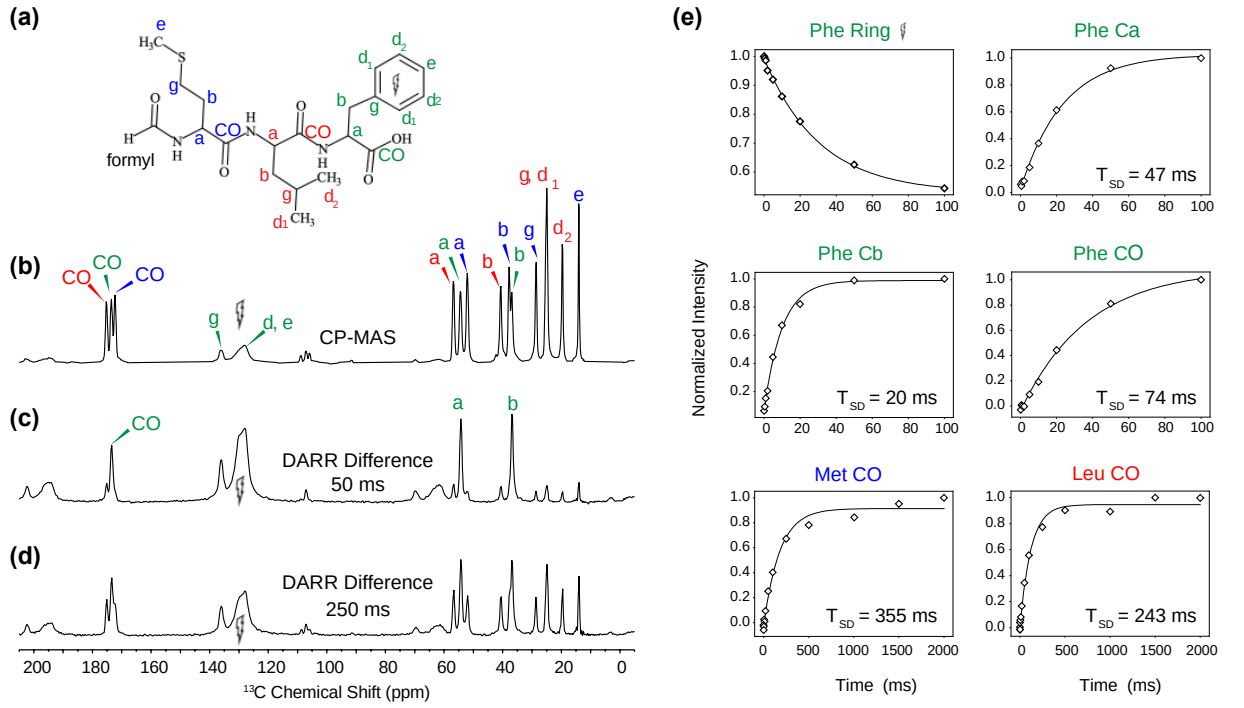

Figure 4. Demonstration of the 1D DARR Difference method applied to ^{13}C-enriched microcrystalline peptide fMLF (150 MHz ^{13}C Larmor frequency, 10 kHz MAS). (a) Chemical structure of fMLF with the carbon sites labeled. (b) ^{13}C 1D CP-MAS spectrum with color-coded spectral assignments. 1D DARR Difference solid-state spectra using Phe ring signal for selection are shown at short (c, 50 ms) and moderate (d, 250 ms) spin-diffusion times. (e) T_1-compensated (Torchia method) spin diffusion buildup curves for select signal, and their extracted spin-diffusion time constants T_{SD}. ^{13}C chemical shifts are relative to DSS at 0.0 ppm (TMS at -2.01 ppm).

1D DARR Difference buildup plots were collected on fMLF at 30 kHz MAS in addition to 10 kHz. Unsurprisingly, ^{1}H-driven ^{13}C-^{13}C spin diffusion rates are attenuated severely at higher spinning frequencies. T_{SD} buildup time constants extracted from Phe aromatic ring-selected 1D data collected at both 10 and 30 kHz MAS frequencies are shown in Table 1. T_{SD} values measured at 30 kHz are likely less accurate than those obtained at 10 kHz (see further discussion in the Supplemental Materials), but the evidence for attenuated spin-diffusion behavior is nevertheless clear. While short-range contacts are easily identified at 30 kHz using the DARR recoupling scheme, longer correlations are much more challenging to observe due to slower buildup kinetics. Results would likely be improved by implementing advanced ^{13}C-^{13}C recoupling methods designed for higher spin rates.[6] For example, the newly-developed Adiabatic Frequency-swept

recoupling scheme AL FRESCO might be an excellent candidate for implementation at moderate and fast spinning speeds.[56] Moreover, we have demonstrated that 1D DARR Difference can be used to quickly obtain detailed performance metrics of various recoupling methods and the effect of spinning speed, which should prove valuable to researchers developing new schemes or choosing between existing ones.

Lignin $S_{1,4}$ to:	Shift (ppm)[a]	T_{SD} (ms)	Distance (nm)
Lignin OMe	56	61	0.36[c]
Lignin Cγ	63	45	0.33[c]
Xylan Ac^{CO}	171	323	0.46 – 0.49[d]
Xylan Ac^{Me}	22	349	0.47 – 0.50[d]

MLF Phe Ring to:	Shift (ppm)[b]	T_{SD} (ms) 10 kHz	T_{SD} (ms) 30 kHz
Phe Cβ	38.9	20	84
Phe Cα	56.4	47	713
Phe CO	175.5	74	1047
Leu CO	177.2	243	3431
Met CO	174.3	355	9087

Table 1. Spin diffusion time constants T_{SD} extracted from T_1-compensated 1D DARR Difference buildup plots for ^{13}C-enriched biomass using Lignin $S_{1,4}$ selection (50 MHz ^{13}C Larmor frequency, 8 kHz MAS), and for microcrystalline peptide fMLF using selection of Phe ring carbons (150 MHz ^{13}C Larmor frequency) at both 10 and 30 kHz MAS rates.

Superscripts in Table 1 denote the following: a) ^{13}C chemical shifts relative to TMS at 0.0 ppm; b) chemical shifts relative to DSS at 0.0 ppm, c) inter-nuclear distance from Molecular Dynamics used as an internal distance candle (see Supplemental Materials) to calibrate ^{13}C-^{13}C spin-diffusion coefficient, and d) measured spin-diffusion coefficient applied to estimate inter-polymer distance.

Sensitivity Enhancement: Selective 1D vs 2D Spin-Diffusion. Significantly improved signal to noise is achieved using the selective 1D spin-diffusion methods compared to the conventional 2D technique. Figure 5 shows 2D ^{13}C-^{13}C DARR spectra obtained on ^{13}C-enriched poplar woody stems and on microcrystalline peptide fMLF. Common practice with these experiments is to extract 1D slices from the 2D plot. Examples of such an extraction taken at 135 ppm for biomass and 131 ppm for fMLF are seen in Figure 5b and 5e, respectively. It is useful to note that the ^{13}C chemical shifts and relative intensities of peaks seen in the 1D slice compares nicely to the 1D

DARR Difference spectra, lending confidence to the selective 1D method as an alternative to the 2D experiment assuming chemical shift selection is possible.

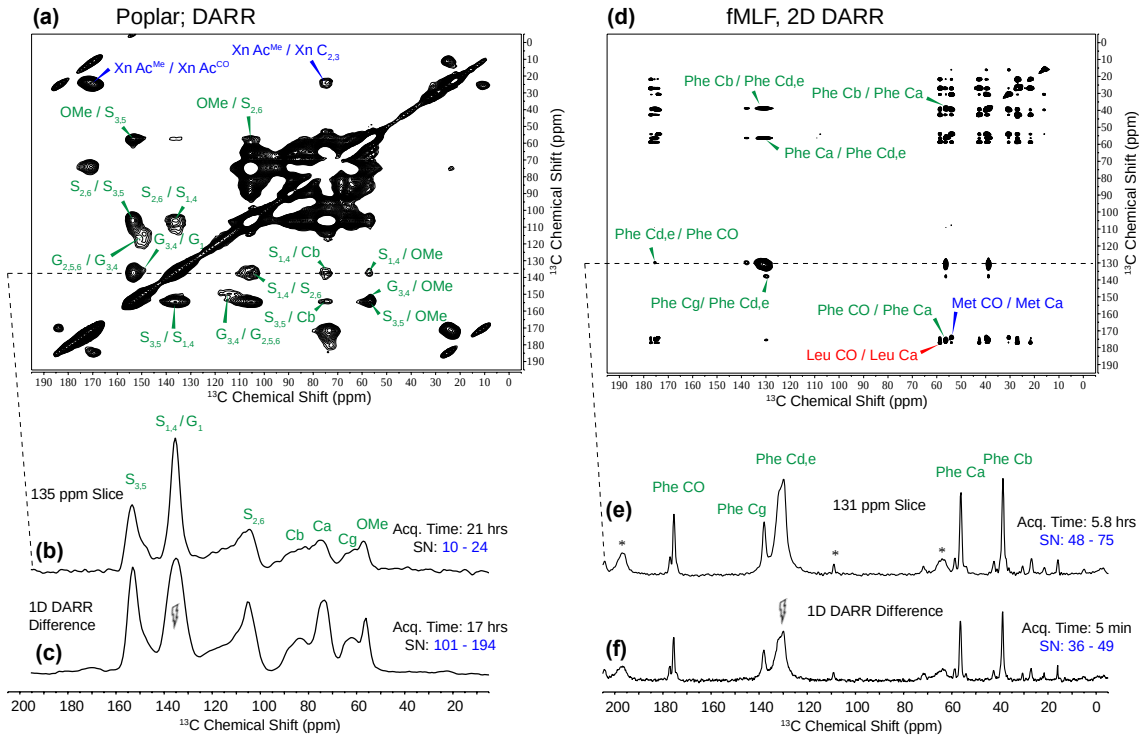

Figure 5. Comparison of traditional 2D DARR data with selective 1D DARR Difference data on ^{13}C-enriched Poplar woody stems (a-c, 50 MHz ^{13}C Larmor frequency, 8 kHz MAS) and microcrystalline peptide fMLF (d-f, 150 MHz ^{13}C Larmor frequency, 10 kHz MAS). Select resonance assignments are indicated and color-coded, and some spinning sidebands are indicated with asterisks. A 1D slice taken at 135 ppm for biomass (b) and 131 ppm for fMLF (e) samples reveal a 1D lignin-selective plot and a 1D Phe-selected plot, respectively, both of which compare nicely to the selective 1D plots.

Signal-to-noise and time savings estimates for various spectra are visualized in Figure 5 and summarized in Table S3. In the case of ^{13}C-enriched Poplar woody stems, both 1D DARR Difference and 2D DARR experiments on ^{13}C-enriched poplar were collected using 20 ms spin-diffusion mixing periods τ_m, with total experiment times of 21 hours for the 2D data (128 scan averages, 192 complex points) and 17 hours for the selective 1D data (20480 scan averages). Even with shorter total experiment time the 1D DARR Difference method boasts roughly 10x improved

S/N ratios compared to the equivalent 1D slice (135 ppm) from the 2D data. Since signal to noise scales as the square root of the number of scans, in order to obtain similar S/N ratios for the 2D method, 80-100x more scans per t1 increment would be required, equating to roughly 2000 hours of spectrometer time. Clearly this is impractical. Interpreted another way, because of the S/N improvement roughly 80-100x less time is required for spatial contact information to be extracted through the 1D method as compared to the full 2D experiment. In other words, short-range contacts within the lignin domain can be extracted in only 10 minutes with similar confidence compared to 21 hours for the 2D method. Naturally, significant information is lost by collapsing 2D data into 1D, therefore selective 1D ^{13}C-^{13}C spin-diffusion methods really only are applicable when ^{13}C chemical shift resolution allows for isolation of a single interested moiety. If spectral overlap remains a problem, or if no resolved moieties exist, 2D methods are preferred. Again, this is analogous to liquid-state NMR selective 1D methods applied routinely to small-molecules.

Instead of collecting data in a shorter timeframe, for ^{13}C-enriched biomass we took advantage of time savings by collecting more than two orders of magnitude more scans for each selective 1D experiment compared to the equivalent 2D experiment. We found this especially useful at very long mixing times since significant loss of signal was observed when the spin-diffusion mixing period was on the order of 1-2x carbon T_1 (T_1 was roughly 3 seconds for all carbons). Importantly, this enabled high confidence in spin-diffusion buildup plots from 1D DARR Difference data even at extremely long (5-7 seconds) mixing times.

For fMLF, the time savings achieved by collapsing the 2D ^{13}C-^{13}C experiment into a selective 1D version are also dramatic. Figure 5d shows a 2D DARR dataset at 50 ms mixing. Data were collected with 16 scans per t_1 increment, a 5 second recycle delay and 256 points in the indirect dimension for a total of 5.8 hours of data collection. At this mixing time 2D ^{13}C-^{13}C cross-peaks

are dominated by short-range interactions, although some inter-residue contacts emerge. A 1D slice taken through the Phe ring region (Figure 5e) effectively shows a selective 1D Phe spectrum, which is virtually identical to the 1D DARR Difference plot obtained using Phe ring selection and the same spin-diffusion mixing period (Figure 5f). The 1D plots are displayed and scaled such that the noise levels are roughly equal. Even though the 1D experiment took ~70x less time compared to the 2D counterpart (5 minutes vs. 5.8 hours), the signal to noise levels are quite comparable; the measured S/N is only one factor of $\sqrt{2}$ less than the 2D slice, meaning the time savings to achieve identical S/N ratios is about 35x (Table S3). Enabled by these time savings, full ^{13}C-^{13}C spin-diffusion buildup experiments on fMLF could be obtained very quickly. We collected 14 1D DARR Difference experiments (Figure 4, Figure S5, Phe ring selection) with mixing periods ranging from very short (100 microseconds) to long (2 seconds). The entire dataset only took about 1.5 hours to collect. An equivalent spin-diffusion buildup dataset using the conventional 2D method would have taken roughly 3.5 days assuming same conditions as the 2D plot in Figure 5d.

We briefly note here that these impressive time savings enabled 1D DARR Difference application at natural abundance (Figure S6). A 20 ms selective 1D experiment was collected on crystalline L-Alanine using carbonyl selection. The data shows clear dipolar contact between the Ala CO peak with Cα and Cβ resonances. Due to the extremely low probability of finding two ^{13}C nuclei spatially close at natural abundance the signal to noise is not good enough to attempt a spin-diffusion buildup array. However, if 1D spin-diffusion methods like 1D DARR Difference or Dante Difference are combined with Dynamic Nuclear Polarization (DNP), the cumulative signal enhancements and time savings may enable informative spin-diffusion buildup experiments on materials at natural abundance.

Application to ^{13}C-enriched Black Widow Spider Dragline Silk. Selective 1D ^{13}C-^{13}C spin-diffusion experiments like Dante Difference and DARR Difference should be broadly applicable to many biopolymer types. To highlight this point, ^{13}C-enriched *Latrodectus hesperus* (Western Black Widow) spider dragline silk was studied to demonstrate how 1D DARR Difference can be applied to amorphous protein-based biomaterials. Black Widow spiders were fed a solution containing U-^{13}C/^{15}N Ala + U-^{13}C/^{15}N Phe, which were metabolized and incorporated into the silk primarily as Ala, Gly, Glu, Ser, and Tyr.[54]

Major ampullate (MA, or dragline) spider silk is a semi-crystalline protein-based biopolymer that boasts outstanding mechanical properties. Dragline silk is roughly five times stronger than steel by weight, is about 35% extensible, and can absorb nearly an order of magnitude more energy per unit mass compared to Kevlar.[80, 81] The unparalleled performance of spider silk is thought to arise from short repetitive protein motifs that comprise over 95% of the total material.[82] For example, Poly(Ala) and Poly(Gly-Ala) motifs aggregate into fiber-aligned anti-parallel β-sheet nanostructures resulting in fiber strength and rigidity, while Gly-rich domains like GPGXX and GGX (X = Tyr, Ala, Gln, Ser) are thought to form disordered helical domains and elastin-like type II β-turns, which contribute to fiber extensibility.[23, 82-85] Much is known about the Ala-rich domains, but Tyr-containing motifs from dragline silks are relatively unstudied. In fact this is the first work detailing Tyr structural analysis within Black Widow dragline silks, although Isdebski studied Tyr-enriched silks from *Nephila clavipes* dragline silks,[86] and the Asakura lab has characterized Tyr residues within silkworm silks and related peptide mimics.[22, 87, 88] One reason for the lack of attention is Tyr comprises less than 5% of all BW dragline silk residues, while Ala and Gly compose 27% and 42%, respectively.[89, 90] Seen clearly in the CP-MAS spectrum in Figure 6b, Tyr Cα, Cβ and CO resonances are buried underneath more dominant signals from Ala, Gly.

To make matters worse, incorporation of enriched amino acids into spider silks typically results in only 20% labeling efficiency.[86, 91] Obtaining ^{13}C chemical shifts from Tyr residues therefore requires 2D methods, or alternatively, here we use 1D DARR Difference to obtain a Tyr-filtered 1D ^{13}C ssNMR spectrum. Tyr-selected 1D spectra (30 kHz MAS) from different spin-diffusion mixing times between 1 ms and 2 seconds are presented in Figure 6a. The key to its utility is that like Dante Difference, DARR Difference method detailed in this work produces in-phase spectra for which only signals directly involved in ^{13}C-^{13}C spin-diffusion with the inverted resonance are observed while all other signals are unobserved. Plots in Figure 6a were scaled by the intensity of the selected Tyr Cδ peak. We find that displaying the selective 1D spectra in this manner is an effective alternative for interpreting buildup data; accurate quantitative analysis of the buildup rates is not possible without proper T_1 compensation but visualizing the data after scaling by the selected peak provides a clear qualitative interpretation.

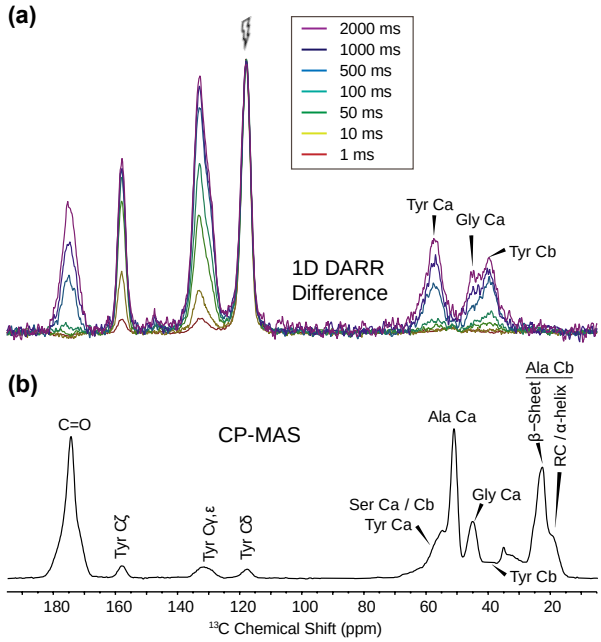

Figure 6. 1D DARR Difference spectra using Tyr Cδ selection collected at a series of increasing mixing times (a) is compared to 1D CP-MAS (b) spectrum on ^{13}C-enriched (U-^{13}C/^{15}N Ala + U-

$^{13}C/^{15}N$ Phe) Black widow spider dragline silk. All data were collected at 30 kHz MAS at 150 MHz ^{13}C Larmor frequency. Spectra are scaled by the Tyr Cδ signal, which allows clean qualitative analysis of the buildup behavior for nearby moieties.

At shorter mixing times (1 - 100 ms), magnetization largely remains within the ring carbons with minor signal emerging at Tyr Cβ, while at longer (500 ms - 2 seconds) mixing times, magnetization transfer has clearly occurred to Tyr Cα, Cβ and CO signals. Additionally, some Gly Cα signal builds in at long mixing times. Since Tyr is most often found in GGY and GPGGY motifs,[89] it is assumed that the emerging Gly signal at 44.5 ppm arises from Gly residues adjacent to Tyr. The slow buildup behavior, which is similar to that of the Tyr CO signal, supports this conclusion. Importantly, observing Tyr/Gly long-range through-space contact was only possible using the selective 1D spin-diffusion method, aided by the ability to collect significantly more scan averages (8192 in this case) and also aided from observing the buildup behavior of the 44.5 ppm shoulder. Spider silk is only sparsely labeled (~20% isotopic enrichment) and Tyr residues only comprise 5% of the total amino acid content. For this reason, we were unable to observe Tyr/Gly correlations using the 2D method, likely because only 128 scan averages could be implemented (Figure S7). From this concept a major benefit of the selective 1D methods like DARR Difference is obvious.

			Predicted Secondary Structure (%)[13, 92]		
Residue	Site	Shift (ppm)	α-helix	Random Coil	β-sheet
Tyr	CO	175.0	8.2	45.8	46.0
	Cα	57.6	13.3	27.0	59.8
	Cβ	39.7	41.6	28.6	29.8
Gly	Cα	44.5	3.7	54.9	41.4

Table 2. Predicted structural probabilities based on ^{13}C chemical shifts obtained from 1D DARR Difference buildup data (Tyr Cδ selection) on ^{13}C-enriched black widow dragline silk. Chemical shifts are referenced DSS.

Chemical shifts were extracted for Tyr Cα, Cβ, CO and Gly Cα signals directly from 1D DARR Difference plots, and are listed in Table 2 along with structural probabilities according to the PLUQin database query.[13, 92] The data suggests that Tyr residues within BW dragline silks adopt

a wide range of structures including disordered random-coil, extended and β-turn structures as indicated by the backbone chemical shifts, but true α-helical structures are much less likely. Supporting this conclusion, based on the Gly Cα chemical shift Gly residues that neighbor Tyr also adopt a range of disordered (random-coil and loosely structured 3_1 helices) and extended conformations but are largely not α-helical.

CONCLUSIONS

The aim of this manuscript is to highlight the underutilized power and broad utility of selective 1D ^{13}C-^{13}C spin-diffusion solid-state NMR methods. Here we apply 1D DARR Difference to a variety of biomaterials including ^{13}C-enriched lignocellulosic biomass, microcrystalline protein standard fMLF, and ^{13}C-enriched Black Widow spider dragline silk. The applicability of selective 1D spin-diffusion methods to probe structural and architectural features of poplar lignocellulosic biomass is emphasized. By collecting spectra at short spin-diffusion times, for the first time we were able to isolate 1D ^{13}C ssNMR spectra for all three major lignocellulosic biomass cell wall polymers from intact material without the need for disruptive chemical or physical treatment procedures. DARR Difference spectra and relaxation-compensated buildup curves targeting lignin aromatic carbons ($S_{1,4}$ / G_1 resonance at 135 ppm) were collected and spin-diffusion behavior was monitored. A key observation is that the ^{13}C-^{13}C spin-diffusion time constant T_{SD} from lignin aromatic carbons to acetylated hemicellulose signals was quite fast at 320-360 ms. This corresponds to a very tight surface interaction with an average internuclear distance of ~0.45 – 0.5 nm between lignin aromatic ring carbons and hemicellulose Ac^{Me} / Ac^{CO} groups. Selective 1D spin-diffusion methods should be applicable to any ^{13}C-enriched material in which chemical-shift selection of unique carbon environments is possible. This concept is demonstrated by its clear

application to probe the molecular structure of Tyr residues within ^{13}C-enriched spider dragline silks. Time savings of the selective 1D method over conventional 2D techniques are discussed. As an example, 1D DARR Difference was applied to the peptide standard fMLF at 10 kHz MAS reveals approximately 35x time savings over the 2D DARR counterpart to extract Phe spin-diffusion interactions, although additional resolution is lost by collapsing the second dimension. Similarly, it was demonstrated that about 10x more signal per unit time (~100x time savings) was achieved for lignin-selected spectra of biomass compared to the 2D DARR. Dante Difference and DARR Difference selection schemes produce selective ^{13}C spectra for which observed ^{13}C signal arises only from carbon sites that are in dipolar contact with a selected resonance. For this reason, these schemes should be of high value as stand-alone methods or as solid-state NMR building blocks for more sophisticated experiments. To name a few examples: Dante Difference has been used in preparation to REDOR dephasing to selectively probe ^{13}C / ^{15}N distances; 1D DARR Difference was shown here to quickly measure the performance of ^{13}C-^{13}C recoupling schemes and compare spin-diffusion dynamics at different spinning rates; the combination of selective 1D with DNP enhancement may prove invaluable for studying polymer spatial arrangements at natural abundance; time-consuming 3D ^{13}C-^{13}C-^{13}C spin-diffusion experiment could be collapsed into a much faster 2D ^{13}C-^{13}C version after chemical-shift selection; and perhaps related shift-edited spin-diffusion methods using ^{19}F or ^{31}P nuclei could be developed. Some of these potential avenues will be explored in future works.

SUPPORTING INFORMATION DESCRIPTION

ASSOCIATED CONTENT

Supporting Information. Chemical shifts of plant cell wall polymers obtained from 1D DARR Difference data; Details for estimating ^{13}C-^{13}C spin-diffusion coefficient and inter-nuclear distance between lignin and hemicellulose; select 1D buildup plots; application at natural abundance; 1D DARR Difference pulse program (Bruker format); instructions for setup.

AUTHOR INFORMATION

Corresponding Author

*Bennett Addison; orcid.org/0000-0003-0763-3137; Email: baddison@nrel.gov

Present Addresses

Notes

The authors declare no competing financial interests. †Designates co-senior author

ACKNOWLEDGMENT

BA designed experiments and wrote the manuscript. DS conducted experiments on spider silk and fMLF. VB performed Molecular Dynamics work. RH and CD prepared enriched biomass for analysis. GPH† and AHW† are considered co-senior authors. All authors contributed vital feedback and revised the manuscript. The authors graciously thank Dr. Mark Davis and Dr. Wellington Muchero for insightful discussions.

This research was supported in part by the U. S. Department of Energy (DOE), Office of Energy Efficiency and Renewable Energy (EERE), Bioenergy Technologies Office (BETO), under Award No. DE-AC36-08GO28308 with the National Renewable Energy Laboratory. Funding was also

provided under The BioEnergy Science Center and The Center for Bioenergy Innovation both a U.S. Department of Energy Research Center supported by the Office of Biological and Environmental Research in the DOE Office of Science. T.W. is supported as part of the Center for Lignocellulose Structure and Formation, an Energy Frontier Research Center funded by the US Department of Energy, Office of Science, Basic Energy Sciences under award number DE-SC0001090. G.P.H. is supported by the US Department of Defense, Air Force Office of Research (DOD-AFOSR) under award number FA9550-17-1-0282 and Army Research Office (DOD-ARO), contract number W911NF2010143. The publisher, by accepting the article for publication, acknowledges that the U. S. Government retains a nonexclusive, paid-up, irrevocable, worldwide license to publish or reproduce the published form of this work, or allow others to do so, for U. S. Government purposes. The views expressed in the article do not necessarily represent the views of the U.S. Department of Energy or the United States Government.

ABBREVIATIONS

SSNMR: Solid State Nuclear Magnetic Resonance

CP-MAS: Cross-Polarization Magic Angle Spinning

DARR: Dipolar-Assisted Rotational Resonance

PDSD: Proton Driven Spin Diffusion

τ_m: spin-diffusion mixing time

S, G, H, FA: syringyl, guaiacyl, p-hydroxyphenyl, ferulate (lignin monomeric units)

Xn: xylan

Ac^{CO}, Ac^{Me}: carbonyl and methyl groups of acetylated xylan

fMLF: microcrystalline peptide standard formyl-Met-Leu-Phe

BW: black widow

REFERENCES

1. Szeverenyi, N.; Sullivan, M.; Maciel, G., Observation of Spin Exchange by Two-Dimensional Fourier Transform 13CCross Polarization-Magic-Angle Spinning. *Journal of Magnetic Resonance* **1982,** *47*, 462-475.
2. Ernst, M.; Meier, B. H., Spin Diffusion in Solids. In *Studies in Physical and Theoretical Chemistry*, Elsevier: 1998; Vol. 84, pp 83-121.
3. Takegoshi, K.; Nakamura, S.; Terao, T., 13C–1H dipolar-assisted rotational resonance in magic-angle spinning NMR. *Chemical Physics Letters* **2001,** *344* (5-6), 631-637.
4. Weingarth, M.; Bodenhausen, G.; Tekely, P., Broadband Carbon-13 Correlation Spectra of Microcrystalline Proteins in Very High Magnetic Fields. *Journal of American Chemical Society* **2009,** *131*, 13937-13939.
5. Weingarth, M.; Demco, D. E.; Bodenhausen, G.; Tekely, P., Improved magnetization transfer in solid-state NMR with fast magic angle spinning. *Chemical Physics Letters* **2009,** *469* (4-6), 342-348.
6. Mithu, V. S.; Bakthavatsalam, S.; Madhu, P. K., 13C-13C Homonuclear Recoupling in Solid-State Nuclear Magnetic Resonance at a Moderately High Magic-Angle- Spinning Frequency. *PLOS ONE* **2013,** *8* (1), 1-10.
7. Hou, G.; Yan, S.; Trébosc, J.; Amoureux, J.-P.; Polenova, T., Broadband homonuclear correlation spectroscopy driven by combined R2nv sequences under fast magic angle spinning for NMR structural analysis of organic and biological solids. *Journal of Magnetic Resonance* **2013,** *232*, 18-30.
8. Grommek, A.; Meier, B. H.; Ernst, M., Distance information from proton-driven spin diffusion under MAS. *Chemical Physics Letters* **2006,** *427* (4-6), 404-409.
9. Suter, D.; Ernst, R. R., Spin diffusion in resolved solid-state NMR spectra. **1995,** *32* (9), 5608-5627.
10. Dumez, J.-N.; Emsley, L., A master-equation approach to the description of proton-driven spin diffusion from crystal geometry using simulated zero-quantum lineshapes. *Phys. Chem. Chem. Phys.* **2011,** (13), 7363-7370.
11. Hong, M.; Schmidt-Rohr, K., Magic-Angle-Spinning NMR Techniques for Measuring Long-Range Distances in Biological Macromolecules. *Acc. Chem. Res.* **2013,** *46* (9), 2154-2163.
12. Lee, W.; Yu, W.; Kim, S.; Chang, I.; Lee, W.; Markley, J. L., PACSY, a relational database management system for protein structure and chemical shift analysis. *Journal of Biomolecular NMR* **2012,** *54* (2), 169-179.
13. Fritzsching, K. J.; Yang, Y.; Schmidt-Rohr, K.; Hong, M., Practical use of chemical shift databases for protein solid-state NMR: 2D chemical shift maps and amino-acid assignment with secondary-structure information. *Journal of Biomolecular NMR* **2013,** *56* (2), 155-167.
14. Wishart, D.; Sykes, B., The 13C Chemical-Shift Index: A simple method for the identification of protein secondary structure using 13C chemical-shift data. *Journal of Biomolecular NMR* **1994,** *4* (2), 171-180.
15. Kang, X.; Zhao, W.; Dickwella Widanage, M. C.; Kirui, A.; Ozdenvar, U.; Wang, T., CCMRD: a solid-state NMR database for complex carbohydrates. *Journal of Biomolecular NMR* **2020,** *74*, 239-245.
16. Manolikas, T.; Herrmann, T.; Meier, B. H., Protein Structure Determination from 13C Spin-Diffusion Solid-State NMR Spectroscopy. *J. Am. Chem. Soc.* **2008,** *130* (12), 3959-3966.

17. Castellani, F.; van Rossum, B.; Diehl, A.; Schubert, M.; Rehbein, K.; Oschkinat, H., Structure of a protein determined by solid-state magic-angle-spinning NMR spectroscopy. *Nature* **2002,** *420* (6911), 99-102.
18. Zech, S. G.; Wand, A. J.; McDermott, A. E., Protein Structure Determination by High-Resolution Solid-State NMR Spectroscopy: Application to Microcrystalline Ubiquitin. *Journal of American Chemical Society* **2005,** (127), 8618-8626.
19. Meier, B. H.; Riek, R.; Böckmann, A., Emerging Structural Understanding of Amyloid Fibrils by Solid-State NMR. *Trends in Biochemical Sciences* **2017,** *42* (10), 777-787.
20. Tycko, R., Progress towards a molecular-level structural understanding of amyloid fibrils. *Current Opinion in Structural Biology* **2004,** *14* (1), 96-103.
21. Tycko, R., Solid-State NMR Studies of Amyloid Fibril Structure. *Annu. Rev. Phys. Chem.* **2011,** *62* (1), 279-299.
22. Asakura, T.; Suzuki, Y.; Nakazawa, Y.; Holland, G. P.; Yarger, J. L., Elucidating silk structure using solid-state NMR. *Soft Matter* **2013,** *9* (48), 11440.
23. Yarger, J. L.; Cherry, B. R.; van der Vaart, A., Uncovering the structure–function relationship in spider silk. *Nat Rev Mater* **2018,** *3* (3), 18008.
24. Opella, S. J.; Marassi, F. M., Structure Determination of Membrane Proteins by NMR Spectroscopy. *Chem. Rev.* **2004,** *104* (8), 3587-3606.
25. Mandala, V. S.; Williams, J. K.; Hong, M., Structure and Dynamics of Membrane Proteins from Solid-State NMR. *Annu. Rev. Biophys.* **2018,** *47* (1), 201-222.
26. Kang, X.; Kirui, A.; Dickwella Widanage, M. C.; Mentink-Vigier, F.; Cosgrove, D. J.; Wang, T., Lignin-polysaccharide interactions in plant secondary cell walls revealed by solid-state NMR. *Nat Commun* **2019,** *10* (1), 347.
27. Wang, T., Multidimensional solid-state NMR spectroscopy of plant cell walls. *Solid State Nuclear Magnetic Resonance* **2016,** *78*, 56-63.
28. Zhao, W.; Fernando, L. D.; Kirui, A.; Deligey, F.; Wang, T., Solid-state NMR of plant and fungal cell walls: A critical review. *Solid State Nuclear Magnetic Resonance* **2020,** *107*, 101660.
29. Kolodziejski, W., Solid-State NMR Studies of Bone. In *New Techniques in Solid-State NMR*, Klinowski, J., Ed. Springer Berlin Heidelberg: Berlin, Heidelberg, 2005; Vol. 246, pp 235-270.
30. Mroue, K. H.; Viswan, A.; Sinha, N.; Ramamoorthy, A., Solid-State NMR Spectroscopy: The Magic Wand to View Bone at Nanoscopic Resolution. In *Annual Reports on NMR Spectroscopy*, Elsevier: 2017; Vol. 92, pp 365-413.
31. Jeener, J.; Meier, B. H.; Bachmann, P.; Ernst, R. R., Investigation of exchange processes by two-dimensional NMR spectroscopy. *The Journal of Chemical Physics* **1979,** *71* (11), 4546-4553.
32. Caravatti, P.; Bodenhausen, G.; Ernst, R. R., Selective pulse experiments in high-resolution solid state NMR. *Journal of Magnetic Resonance (1969)* **1983,** *55* (1), 88-103.
33. Dalvit, C., New One-Dimensional Selective NMR Experiments in Aqueous Solutions Recorded with Pulsed Field Gradients. *Journal of Magnetic Resonance, Series A* **1995,** *113* (1), 120-123.
34. Kessler, H.; Oschkinat, H.; Griesinger, C.; Bermel, W., Transformation of homonuclear two-dimensional NMR techniques into one-dimensional techniques using Gaussian pulses. *Journal of Magnetic Resonance (1969)* **1986,** *70* (1), 106-133.

35. Hu, H.; Bradley, S. A.; Krishnamurthy, K., Extending the limits of the selective 1D NOESY experiment with an improved selective TOCSY edited preparation function. *Journal of Magnetic Resonance* **2004,** *171* (2), 201-206.
36. Bodenhausen, G.; Freeman, R.; Morris, G. A., A simple pulse sequence for selective excitation in Fourier transform NMR. *Journal of Magnetic Resonance (1969)* **1976,** *23* (1), 171-175.
37. Masuda, K.; Adachi, M.; Hirai, A.; Yamamoto, H.; Kaji, H.; Horii, F., Solid-state 13C and 1H spin diffusion NMR analyses of the microfibril structure for bacterial cellulose. *Solid State Nuclear Magnetic Resonance* **2003,** *23* (4), 198-212.
38. Tekely, P.; Brondeau, J.; Elbayed, K.; Retournard, A.; Canet, D., A simple pulse train, using 90° hard pulses, for selective excitation in high-resolution solid-state NMR. *Journal of Magnetic Resonance (1969)* **1988,** *80* (3), 509-516.
39. Foston, M.; Katahira, R.; Gjersing, E.; Davis, M. F.; Ragauskas, A. J., Solid-State Selective 13C Excitation and Spin Diffusion NMR To Resolve Spatial Dimensions in Plant Cell Walls. *J. Agric. Food Chem.* **2012,** *60* (6), 1419-1427.
40. Bork, V.; Schaefer, J., Measuring 13C-13C connectivity in spinning solids by selective excitation. *Journal of Magnetic Resonance (1969)* **1988,** *78* (2), 348-354.
41. Kim, S. J.; Chang, J.; Rimal, B.; Yang, H.; Schaefer, J., Surface proteins and the formation of biofilms by Staphylococcus aureus. *Biochimica et Biophysica Acta (BBA) - Biomembranes* **2018,** *1860* (3), 749-756.
42. Yang, H.; Singh, M.; Kim, S. J.; Schaefer, J., Characterization of the tertiary structure of the peptidoglycan of Enterococcus faecalis. *Biochimica et Biophysica Acta (BBA) - Biomembranes* **2017,** *1859* (11), 2171-2180.
43. Auchus, R. J.; Covey, D. F.; Borkll, V.; Schaeferll, J., Solid-state NMR Observation of Cysteine andLysine Michael Adducts of Inactivated Estradiol Dehydrogenase. *The Journal of Biological Chemistry* **1988,** *263* (24), 11640-11645.
44. Kim, S. J.; Singh, M.; Sharif, S.; Schaefer, J., Cross-Link Formation and Peptidoglycan Lattice Assembly in the FemA Mutant of Staphylococcus aureus. *Biochemistry* **2014,** *53* (9), 1420-1427.
45. Cegelski, L.; Schaefer, J., Glycine Metabolism in Intact Leaves by in Vivo 13C and 15N Labeling. *J. Biol. Chem.* **2005,** *280* (47), 39238-39245.
46. Veshtort, M.; Griffin, R. G., High-Performance Selective Excitation Pulses for Solid- and Liquid-State NMR Spectroscopy. *ChemPhysChem* **2004,** *5* (6), 834-850.
47. Li, Y.; Wylie, B. J.; Rienstra, C. M., Selective refocusing pulses in magic-angle spinning NMR: Characterization and applications to multi-dimensional protein spectroscopy. *Journal of Magnetic Resonance* **2006,** *179* (2), 206-216.
48. Theimer, D.; Bodenhausen, G., Shaped pulses for selective inversion of magnetization in solids spinning at the magic angle. *Appl. Magn. Reson.* **1992,** *3* (6), 981-998.
49. Weber, D. K.; Bader, T.; Larsen, E. K.; Wang, S.; Gopinath, T.; Distefano, M.; Veglia, G., Cysteine-ethylation of tissue-extracted membrane proteins as a tool to detect conformational states by solid-state NMR spectroscopy. In *Methods in Enzymology*, Elsevier: 2019; Vol. 621, pp 281-304.
50. Emsley, L.; Bodenhausen, G., Gaussian pulse cascades: New analytical functions for rectangular selective inversion and in-phase excitation in NMR. *Chemical Physics Letters* **1990,** *165* (6), 469-476.

51. Morcombe, C. R.; Zilm, K. W., Chemical shift referencing in MAS solid state NMR. *Journal of Magnetic Resonance* **2003,** *162* (2), 479-486.
52. Torchia, D. A., The measurement of proton-enhanced carbon-13 T1 values by a method which suppresses artifacts. *Journal of Magnetic Resonance (1969)* **1978,** *30* (3), 613-616.
53. Work, R. W.; Emerson, P. D., An Apparatus and Technique for the Forcible Silking of Spiders. *J. Arachnol.* **1982,** *10* (1), 1-10.
54. Creager, M. S.; Izdebski, T.; Brooks, A. E.; Lewis, R. V., Elucidating metabolic pathways for amino acid incorporation into dragline spider silk using 13C enrichment and solid state NMR. *Comparative Biochemistry and Physiology Part A: Molecular & Integrative Physiology* **2011,** *159* (3), 219-224.
55. Geen, H.; Freeman, R., Band-selective radiofrequency pulses. *Journal of Magnetic Resonance (1969)* **1991,** *93* (1), 93-141.
56. Wi, S.; Frydman, L., An Efficient, Robust New Scheme for Establishing Broadband Homonuclear Correlations in Biomolecular Solid State NMR. *ChemPhysChem* **2020,** *21* (4), 284-294.
57. Lu, X.; Guo, C.; Hou, G.; Polenova, T., Combined zero-quantum and spin-diffusion mixing for efficient homonuclear correlation spectroscopy under fast MAS: broadband recoupling and detection of long-range correlations. *Journal of Biomolecular NMR* **2015,** *61* (1), 7-20.
58. Terrett, O. M.; Lyczakowski, J. J.; Yu, L.; Iuga, D.; Franks, W. T.; Brown, S. P.; Dupree, R.; Dupree, P., Molecular architecture of softwood revealed by solid-state NMR. *Nat Commun* **2019,** *10* (1), 4978.
59. Simmons, T. J.; Mortimer, J. C.; Bernardinelli, O. D.; Pöppler, A.-C.; Brown, S. P.; deAzevedo, E. R.; Dupree, R.; Dupree, P., Folding of xylan onto cellulose fibrils in plant cell walls revealed by solid-state NMR. *Nat Commun* **2016,** *7* (1), 13902.
60. Dupree, R.; Simmons, T. J.; Mortimer, J. C.; Patel, D.; Iuga, D.; Brown, S. P.; Dupree, P., Probing the Molecular Architecture of Arabidopsis thaliana Secondary Cell Walls Using Two- and Three-Dimensional 13C Solid State Nuclear Magnetic Resonance Spectroscopy. *Biochemistry* **2015,** *54* (14), 2335-2345.
61. Kirui, A.; Ling, Z.; Kang, X.; Dickwella Widanage, M. C.; Mentink-Vigier, F.; French, A. D.; Wang, T., Atomic resolution of cotton cellulose structure enabled by dynamic nuclear polarization solid-state NMR. *Cellulose* **2019,** *26* (1), 329-339.
62. Yoo, C. G.; Dumitrache, A.; Muchero, W.; Natzke, J.; Akinosho, H.; Li, M.; Sykes, R. W.; Brown, S. D.; Davison, B.; Tuskan, G. A.; Pu, Y.; Ragauskas, A. J., Significance of Lignin S/G Ratio in Biomass Recalcitrance of Populus trichocarpa Variants for Bioethanol Production. *ACS Sustainable Chem. Eng.* **2018,** *6* (2), 2162-2168.
63. Sannigrahi, P.; Ragauskas, A. J.; Tuskan, G. A., Poplar as a feedstock for biofuels: A review of compositional characteristics. *Biofuels, Bioprod. Bioref.* **2010,** *4* (2), 209-226.
64. Anderson, E. M.; Stone, M. L.; Katahira, R.; Reed, M.; Muchero, W.; Ramirez, K. J.; Beckham, G. T.; Román-Leshkov, Y., Differences in S/G ratio in natural poplar variants do not predict catalytic depolymerization monomer yields. *Nat Commun* **2019,** *10* (1), 2033.
65. Carpita, N. C.; Gibeaut, D. M., Structural models of primary cell walls in flowering plants: consistency of molecular structure with the physical properties of the walls during growth. *Plant J* **1993,** *3* (1), 1-30.

66. McCann, M. C.; Roberts, K.; Wilson, R. H.; Gidley, M. J.; Gibeaut, D. M.; Kim, J.-B.; Carpita, N. C., Old and new ways to probe plant cell-wall architecture. *Can. J. Bot.* **1995,** *73* (S1), 103-113.
67. da Costa Sousa, L.; Chundawat, S. P. S.; Balan, V.; Dale, B. E., 'Cradle-to-grave' assessment of existing lignocellulose pretreatment technologies. *Current Opinion in Biotechnology* **2009,** *20* (3), 339-347.
68. Zakzeski, J.; Bruijnincx, P. C. A.; Jongerius, A. L.; Weckhuysen, B. M., The Catalytic Valorization of Lignin for the Production of Renewable Chemicals. *Chem. Rev.* **2010,** *110* (6), 3552-3599.
69. Ragauskas, A. J.; Beckham, G. T.; Biddy, M. J.; Chandra, R.; Chen, F.; Davis, M. F.; Davison, B. H.; Dixon, R. A.; Gilna, P.; Keller, M.; al, e., Lignin Valorization: Improving Lignin Processing in the Biorefinery. *Science* **2014,** *344* (6185), 1246843-1246843.
70. Harman-Ware, A. E.; Crocker, M.; Pace, R. B.; Placido, A.; Morton, S.; DeBolt, S., Characterization of Endocarp Biomass and Extracted Lignin Using Pyrolysis and Spectroscopic Methods. *Bioenerg. Res.* **2015,** *8* (1), 350-368.
71. Yang, H.; Yoo, C. G.; Meng, X.; Pu, Y.; Muchero, W.; Tuskan, G. A.; Tschaplinski, T. J.; Ragauskas, A. J.; Yao, L., Structural changes of lignins in natural Populus variants during different pretreatments. *Bioresource Technology* **2020,** *295*, 122240.
72. Manders, W. F., Solid-State 13C NMR Determination of the Syringyl/Guaiacyl Ratio in Hardwoods. *Holzforschung* **1987,** *41* (1), 13-17.
73. Nimz, H. H.; Robert, D.; Faix, O.; Nemr, M., Carbon-13 NMR Spectra of Lignins, 8. Structural Differences between Lignins of Hardwoods, Softwoods, Grasses and Compression Wood. *Holzforschung* **1981,** *35* (1), 16-26.
74. Lapierre, C.; Monties, B.; Guittet, E.; Lallemand, J. Y., Photosynthetically 13C-Labelled Poplar Lignins: - 13C NMR Experiments. *Holzforschung* **1984,** *38* (6), 333-342.
75. Kim, H.; Ralph, J., Solution-state 2D NMR of ball-milled plant cell wall gels in DMSO-d6/pyridine-d5. *Org. Biomol. Chem.* **2010,** *8* (3), 576-591.
76. Wen, J.-L.; Sun, S.-L.; Xue, B.-L.; Sun, R.-C., Recent Advances in Characterization of Lignin Polymer by Solution-State Nuclear Magnetic Resonance (NMR) Methodology. *Materials* **2013,** *6* (1), 359-391.
77. Wang, T.; Williams, J. K.; Schmidt-Rohr, K.; Hong, M., Relaxation-compensated difference spin diffusion NMR for detecting 13C–13C long-range correlations in proteins and polysaccharides. *Journal of Biomolecular NMR* **2015,** *61* (2), 97-107.
78. Bromley, J. R.; Busse-Wicher, M.; Tryfona, T.; Mortimer, J. C.; Zhang, Z.; Brown, D. M.; Dupree, P., GUX1 and GUX2 glucuronyltransferases decorate distinct domains of glucuronoxylan with different substitution patterns. *Plant J* **2013,** *74* (3), 423-434.
79. Busse-Wicher, M.; Gomes, T. C. F.; Tryfona, T.; Nikolovski, N.; Stott, K.; Grantham, N. J.; Bolam, D. N.; Skaf, M. S.; Dupree, P., The pattern of xylan acetylation suggests xylan may interact with cellulose microfibrils as a twofold helical screw in the secondary plant cell wall of Arabidopsis thaliana. *Plant J* **2014,** *79* (3), 492-506.
80. Gosline, J. M.; DeMont, M. E.; Denny, M. W., The structure and properties of spider silk. *Endeavour* **1986,** *10* (1), 37-43.
81. Griffiths, J. R.; Salanitri, V. R., The strength of spider silk. *J Mater Sci* **1980,** *15* (2), 491-496.

82. Hayashi, C. Y.; Shipley, N. H.; Lewis, R. V., Hypotheses that correlate the sequence, structure, and mechanical properties of spider silk proteins. *International Journal of Biological Macromolecules* **1999,** *24* (2-3), 271-275.
83. Jenkins, J. E.; Creager, M. S.; Butler, E. B.; Lewis, R. V.; Yarger, J. L.; Holland, G. P., Solid-state NMR evidence for elastin-like β-turn structure in spider dragline silk. *Chem. Commun.* **2010,** *46* (36), 6714.
84. Tokareva, O.; Jacobsen, M.; Buehler, M.; Wong, J.; Kaplan, D. L., Structure–function–property–design interplay in biopolymers: Spider silk. *Acta Biomaterialia* **2014,** *10* (4), 1612-1626.
85. Xu, M.; Lewis, R. V., Structure of a protein superfiber: spider dragline silk. *Proc Natl Acad Sci USA* **1990,** *87* (18), 7120-7124.
86. Izdebski, T.; Akhenblit, P.; Jenkins, J. E.; Yarger, J. L.; Holland, G. P., Structure and Dynamics of Aromatic Residues in Spider Silk: 2D Carbon Correlation NMR of Dragline Fibers. *Biomacromolecules* **2010,** *11* (1), 168-174.
87. Asakura, T.; Suita, K.; Kameda, T.; Afonin, S.; Ulrich, A. S., Structural role of tyrosine in Bombyx mori silk fibroin, studied by solid-state NMR and molecular mechanics on a model peptide prepared as silk I and II: Solid-state NMR of tyrosine in silk peptide. *Magn. Reson. Chem.* **2004,** *42* (2), 258-266.
88. Asakura, T.; Sugino, R.; Yao, J.; Takashima, H.; Kishore, R., Comparative Structure Analysis of Tyrosine and Valine Residues in Unprocessed Silk Fibroin (Silk I) and in the Processed Silk Fiber (Silk II) from Bombyx mori Using Solid-State 13C, 15N, and 2H NMR†. *Biochemistry* **2002,** *41* (13), 4415-4424.
89. Ayoub, N. A.; Garb, J. E.; Tinghitella, R. M.; Collin, M. A.; Hayashi, C. Y., Blueprint for a High-Performance Biomaterial: Full-Length Spider Dragline Silk Genes. *PLoS ONE* **2007,** *2* (6), e514.
90. Casem, M. L.; Turner, D.; Houchin, K., Protein and amino acid composition of silks from the cob weaver, Latrodectus hesperus (black widow). *International Journal of Biological Macromolecules* **1999,** *24* (2-3), 103-108.
91. Shi, X.; Yarger, J. L.; Holland, G. P., Probing site-specific 13C/15N-isotope enrichment of spider silk with liquid-state NMR spectroscopy. *Anal Bioanal Chem* **2013,** *405* (12), 3997-4008.
92. Fritzsching, K. J.; Hong, M.; Schmidt-Rohr, K., Conformationally selective multidimensional chemical shift ranges in proteins from a PACSY database purged using intrinsic quality criteria. *Journal of Biomolecular NMR* **2016,** *64* (2), 115-130.